Design of Radiation Tolerant Materials Via Interface Engineering

Submitted to ADVANCED MATERIALS

DOI: 10.1002/adma.((201303400))
Article type: Communication

Design of Radiation Tolerant Materials via Interface Engineering

Weizhong Han, Michael J. Demkowicz, Nathan A. Mara, Engang Fu, Subhasis Sinha, Anthony D. Rollett, Yongqiang Wang, John S. Carpenter, Irene J. Beyerlein, Amit Misra*

Drs W.Z. Han*, N.A. Mara, E.G. Fu, Y.Q. Wang, J.S. Carpenter, I.J. Beyerlein, A. Misra
Los Alamos National Laboratory, Los Alamos, NM 87545, USA
E-mail: wzhanmail@gmail.com or Weizhong@lanl.gov

Prof. M.J. Demkowicz
Department of Materials Science and Engineering, Massachusetts Institute of Technology, Cambridge, MA 02139, USA

Mr. S. Sinha, Prof. A.D. Rollet
Department of Materials Science and Engineering, Carnegie Mellon University, Pittsburgh, PA 15213, USA

Keywords: ((irradiation tolerance, interface, sink efficiency, nanocomposite, thermal stability))

The core of a nuclear reactor presents exceptionally stringent requirements for structural materials due to its high temperature and intense radiation as well as its need for unfailing mechanical integrity[1-4]. Thus, candidate materials for nuclear applications must possess excellent irradiation tolerance, high strength, and thermal stability. However, these properties are difficult to realize simultaneously in one material because of apparently intrinsic tradeoffs between them. Here we report a novel interface engineering strategy that simultaneously achieves superior irradiation tolerance, high strength, and high thermal stability in bulk nanolayered (NL) Cu-Nb composites. By synthesizing bulk NL Cu-Nb composites containing interfaces with controlled sink efficiencies, we design a material in which nearly all irradiation-induced defects are

annihilated. In contrast to grain boundaries in single-phase metals, the Cu-Nb interfaces in these composites remain stable and void free. Interface engineered bulk NL composites are adaptable to large-scale industrial production and exemplify an innovative approach to design interface-dominated materials that eliminate the trade-offs that constrain conventional alloy design.

Coarse-grained polycrystals are thermally stable, but generally mechanically weak and susceptible to radiation-induced swelling, hardening, and embrittlement[5-9]. Nanocrystalline (NC) materials have high strength[10-14] and improved radiation resistance[15,16] because of their high density of grain boundaries (GBs), which are sinks for irradiation-induced defects[17-20] and obstacles for mobile dislocations[10-14]. Nevertheless, most NC materials are not thermally stable and coarsen rapidly even at modest temperatures[21,22]. Recently, nanotwinned metals were shown to have both high strength and thermal stability[23-25]. However, these materials do not have increased radiation resistance because they contain mostly coherent twin boundaries (CTB), which are poor traps for radiation-induced defects[20].

Similar to GBs in NC solids, interfaces play a major role in determining the properties of NL composites[4]. Moreover, interfaces of differing crystallography or composition possess distinct properties, including sink efficiencies for radiation-induced defects[20,26]. They, therefore, provide additional parameters for materials design, beyond grain size and composition alone: parameters that may be used to impart to nanocomposites properties that are not otherwise simultaneously realizable in one material.

Bulk NL Cu-Nb composites with ultrahigh hardness (H_v=4.13±0.4 GPa), tensile strength (σ=1 GPa), and excellent thermal stability[27-30] have recently been fabricated through accumulative roll bonding (ARB)[31,32]. These materials may be processed as sheets of area

approaching 1m^2 and total thickness of several millimeters while the individual layers making up the composite are as thin as ~10 nm. Furthermore, bulk NL Cu-Nb composites contain a narrow distribution of special interface types, primarily Cu{112}<110>//Nb{112}<111> and secondly Cu{110}<110>//Nb{112}<111>[27-30]. Many of these interfaces are atomically faceted and differ from the atomically flat interfaces found in NL Cu-Nb composites synthesized by physical vapor deposition (PVD), where Cu{111}<110>//Nb{110}<111>[4]. The unique interfaces formed in bulk NL Cu-Nb composites may lead to unprecedented irradiation resistance. We use bulk NL Cu-Nb composites as a model system to explore the irradiation tolerance of interface engineered materials with a view towards later adapting the same design principles to more reactor-relevant compositions.

To investigate the radiation response of NL Cu-Nb composites, we directly radiated transmission electron microscopy (TEM) foils of ARB Cu-Nb composites using He ions at 450°C (Figure. S1). The incident He ions pass completely through the foils, but create a uniform damage level of ~3 dpa in both Cu and Nb layers (Figure. S2). **Figure. 1** and S3 show a typical cross-section TEM image of an irradiated ARB NL Cu-Nb composite with individual layer thickness of 135 nm. The original layered morphology of the as-processed state remains unchanged by the 6h, 450°C irradiation, confirming excellent thermal stability.

Comparison of the selected area diffraction patterns (SADP) for as-processed (Figure. S3b) and irradiated (Figure. S3c) samples show that the Nb diffraction spots have broadened due to the large number of vacancies created by irradiation in the Nb layers while the Cu diffraction spots are unchanged. This difference is due to unlike vacancy mobilities, which, at 450°C, are much higher in Cu (T=0.41$T_{m\text{-}Cu}$ and ΔE_v^m=0.69 eV) than in

Nb ($T=0.18T_{m\text{-}Nb}$ and ΔE_v^m=1 eV)[33]. Self-interstitials, on the other hand, are highly mobile at this temperature in both Cu and Nb. Due to their higher mobility, some of the radiation-induced vacancies in Cu layers recombine with interstitials, while others migrate to nearby sinks, which may be Cu-Nb interfaces, Cu GBs, voids, or free surfaces. Consequently, the steady-state number density of radiation-induced vacancies in Cu is low, leading to less lattice distortion than in Nb.

As radiation-induced vacancies diffuse in Cu layers, some of them cluster and eventually form voids, which are a classical form of damage in irradiated metals[5,18]. Numerous voids of ~5 nm diameter may be found in Cu layers at the end of the irradiation experiment, as shown in Figure. 1a. Consistent with the low mobility of Nb vacancies, no voids are seen in the Nb layers. Unlike GBs in pure Cu[20], Cu-Nb interfaces are not decorated with voids after irradiation. The number density of voids within individual Cu layers may be measured as a function of distance from the neighboring interfaces by dividing the layer into several parallel slices (Figure. 1b) and counting the voids in each slice. Figure 1c shows that the density of voids is highest in the middle of the layer and decreases in the regions closest to the Cu-Nb interfaces. Distinct void-denuded zones (VDZs) are present near the Cu-Nb interfaces. These zones are a direct consequence of the diffusion of radiation-induced vacancies to and their subsequent trapping at Cu-Nb interfaces. They demonstrate that interfaces may heal radiation damage.

VDZ widths differ from interface to interface. For example, the void density at interface I in Figure. 1b is lower than the one at interface II, indicating larger VDZ at interface I than at interface II. This variability is the evidence that different Cu-Nb interfaces are vacancy sinks of differing efficiency. Previous investigations have demonstrated that the sink efficiency of GBs in pure Cu depends on their complete crystallographic character[20].

Similarly, the present investigation shows that the sink efficiency of Cu-Nb interfaces is a function of interface crystallographic character.

We used precession electron diffraction (PED)[34] to determine the crystallographic character of sixteen distinct Cu-Nb interfaces. The PED scan is conducted over a region containing several interfaces, such as that shown in **Figure. 2**a, yielding the complete orientation map, as in Figure. 2b. The character of each interface, expressed as the interface plane normal and image normal, for both phases may be determined. For example, the interface marked in Figure. 2c has a character of Cu(11 2 $\overline{11}$)[8 9 7]//Nb($\bar{8}$ 19 $\bar{8}$)[19 19 23]. The crystallographic characters of all the interfaces we studied are listed in Table S1 and related to bulk texture in ARB NL Cu-Nb composites in Figure. S4.

Figure 3a compares the VDZ widths measured here with ones found after identical irradiation experiments near GBs in pure Cu[20] as well as near PVD Cu-Nb interfaces. The sink efficiency of ARB NL Cu-Nb interfaces is smaller than those of non-Σ3 GBs in Cu, comparable to incoherent Σ3 GBs in Cu, and greater than PVD NL Cu-Nb interfaces. However, an important qualitative difference between all the irradiated Cu-Nb interfaces and GBs in pure Cu is that, after irradiation, the latter become decorated with numerous voids[20]. GB voids are deleterious to GB mechanical integrity and play a central role in their eventual mechanical failure[35]. By contrast, there are no voids at all along either the ARB or PVD NL Cu-Nb interfaces, indicating these interfaces are not as susceptible to the radiation-induced mechanical degradation that affects GBs in pure Cu.

Figure 3b sorts all the interfaces investigated here into groups according to their Cu terminal planes and lists their VDZ widths. Group I, with Cu terminal planes near {112}, has highest VDZ widths. Group II contains interfaces with Cu interface plane near {110} and has slightly lower sink efficiency than Group I. Group III contains interfaces that have Cu

terminal planes near neither {112} nor {110}. Due to the particular texture of ARB NL Cu-Nb composites[28], there are far fewer group III interfaces than in groups I or II. Their VDZ widths are highly variable.

Notably, of all the ARB NL Cu-Nb interfaces, the ones with Cu {112} and Nb {112} terminal planes have the greatest sink efficiency. For example, Figure. 3c and d show over- and under-focus images (where voids show up as darker or lighter contrast, respectively) of an irradiated interface whose crystallographic character, Cu(10 25 $\overline{13}$)[20 4 23]//Nb($\overline{13}$ 7 6)[$\overline{12}$ $\overline{11}$ $\overline{14}$], matches closely with Cu{112}<110>//Nb{112}<111>. Interestingly, interfaces of this type have low energies compared to others and contain a distinctive arrangement of misfit dislocations whose Burgers vectors have components pointing out of the interface plane[36,37].

These findings suggest the following strategy for synthesizing radiation-resistant ARB NL Cu-Nb composites: maximize the number of Cu{112}<110>//Nb{112}<111> interfaces and reduce the thickness of individual layers to 40 nm or less. In such composites, the 10~20 nm-wide VDZs of adjacent interfaces would overlap and, therefore, all the Cu layers may be expected to be free of radiation-induced voids. Additionally, the total area of Cu GBs would also be reduced, attenuating any degradation modes that may occur there. To reduce layer thicknesses below 40 nm, the ARB NL Cu-Nb composites with 135 nm layer thicknesses must be subjected to further rolling reduction. To maximize the number of Cu{112}<110>//Nb{112}<111> interfaces, we make use of the intrinsic texture evolution of ARB NL Cu-Nb composite under rolling. This texture evolution depends on the rolling directions applied in successive rolling passes and favors the formation of Cu{112}<110>//Nb{112}<111> interfaces when all successive rolling passes are made while keeping the rolling direction fixed[27-29].

Applying this strategy, we synthesized ARB NL Cu-Nb composites with individual layer thicknesses of ~20 nm and containing a large portion of Cu{112}<110>//Nb{112}<111> interfaces[27-29]. TEM images of these composites after irradiation shown in **Figure. 4**a and S5 demonstrate that their original layered morphology survived the irradiation intact, confirming excellent thermal stability. Figure. 4a demonstrates that the Cu layers are indeed nearly completely void-free. Only small, isolated voids may be found, mostly in the thickest layers. We have counted the number density of the voids in the finer layers and plotted it in Fig. 1c. Both the number density and size of voids in the finer layers is markedly reduced compared to the 135 nm ARB NL Cu-Nb composites. Most significantly, no voids were seen on any of the Cu-Nb interfaces.

For comparison, we synthesized pure NC Cu film with grains of ~20 nm diameter using PVD and subjected it to identical irradiation. Figure 4b shows the outcome of this experiment. The grain size in NC Cu coarsened to diameters of ~60 nm during the irradiation, corresponding to a three-fold reduction in the total GB area per unit volume. The grain interiors are indeed mostly free of voids, but the GBs themselves contain numerous and relatively large voids, which have a deleterious effect on the mechanical integrity of the NC Cu film.

These results illustrate a dramatic contrast between interface-engineered materials, such as ARB NL Cu-Nb composites, and materials processed by conventional methods, such as NC Cu. While both materials initially exhibit significantly enhanced mechanical strength due to their nanometer-scale microstructural dimensions[10-14,28], the interface-engineered material retains this enhanced strength due to its thermal stability while the NC Cu progressively loses it as it coarsens[21,22]. Similarly, while both materials show a reduction in the number of radiation-induced voids in grain interiors due to the

absorption of radiation-induced vacancies at interfaces and GBs, the engineered interfaces in the ARB NL Cu-Nb composites remain void-free and therefore mechanically sound while the GBs in NC Cu are severely damaged by irradiation. Therefore, the interface-engineered material is radiation resistant, mechanically strong, and thermally stable while the conventional NC material is not.

Our findings demonstrate that properties that might not be simultaneously achievable in one material by conventional materials design—such as strength, stability, and radiation resistance—may be realized simultaneously through interface engineering. From a technical standpoint, integrating interface engineering and severe plastic deformation techniques provides a new and industrially relevant route for controlled manufacturing of composites. Expanding this design space to include other composite morphologies, compositions, and interface types, may enable the synthesis of materials that simultaneously exhibit additional properties that have hitherto appeared to be mutually exclusive.

Experimental Section

Fabrication of Cu-Nb composites by accumulative roll bonding (ARB)

ARB NL Cu-Nb composites were fabricated using repeated rolling, cutting, stacking, and further rolling. The process began with one plate of polycrystalline reactor grade Nb (99.97% purity) and two plates of oxygen-free high conductivity Cu (99.99% purity) with a thickness of 1 mm and 0.5 mm respectively, length of 20 cm, and width of 6.5 cm. To promote bonding, the surfaces were cleaned ultrasonically for five-minutes in an acetone bath followed by wire brushing. Roll bonding was performed at room temperature with a ~50% reduction in thickness. Finally, the sample was cut in half and the process described

above was repeated. Each iteration resulted in a doubling of the number of layers in the composite and halving of their thickness. After the thickness of individual layers reached 200 nm, only the rolling step was performed with no re-stacking, decreasing the overall sample thickness. Through this process, composites with individual layers from several hundred micrometers down to 10 nm were fabricated. The *average* values of the layer thickness were estimated based on the number of layers and the overall sample thickness. In this study, we used ARB NL Cu-Nb samples with average layer thickness of 135 nm and 20 nm.

Irradiation experimental design

We introduced radiation damage into ARB NL Cu-Nb composites using a He ion beam, as shown in Fig. S1. The goal of our experiments was to observe how the clustering of radiation-induced vacancies is affected by the proximity of Cu-Nb interfaces without interference from any implanted ions. Therefore, the energy of the ion beam was chosen to be high enough so that nearly all incident ions passed through our samples. He depth profiles computed using SRIM[38] for a He ion energy of 200 keV incident on pure Cu and pure Nb are shown in Fig. S2. In these cases, the implanted He concentration is near zero in the first ~150 nm adjacent to the free surface, but the radiation damage level (expressed in displacements per atom—dpa) is nearly constant. Therefore, we prepared ~100nm-thick cross-section TEM (XTEM) samples first using conventional methods and performed He irradiation directly on these foils. According to the SRIM calculations shown in Fig. S2, incident He ions pass entirely through the electron-transparent regions (less than 100 nm) in XTEM samples and the implanted He concentration in them is negligible while the irradiation damage is almost uniform, with a value of ~3 dpa. Irradiations were performed at 450°C over 6h to a fluence of $2x10^{17}$ ions/cm^2 at the Ion

Beam Materials Laboratory at Los Alamos National Laboratory. Stage temperature was monitored with a thermocouple and remained within ±10°C of the pre-set value.

Microstructure characterization

Irradiated XTEM samples were examined using a Tecnai F30 operated at 300 keV with a field emission gun. A series of irradiation damage features were imaged using two-beam diffraction contrast as well as with defocus of ±2 μm or ±3 μm. To determine interface orientation relationships, a region containing the interface of interest was identified in TEM and a low-magnification image was recorded. This region was then scanned using precession electron diffraction (PED) with a step size of 5 nm or 20 nm for ARB Cu-Nb specimens with an average layer thickness of 20 nm or 135 nm, respectively. Using these methods, we can accurately correlate irradiation damage features with the character of the interface of interest.

Supporting Information

Supporting Information is available online from the Wiley Online Library or from the author.

Acknowledgements

This work was supported by the Center for Materials in Irradiation and Mechanical Extremes (CMIME), an Energy Frontier Research Center (EFRC) funded by the US Department of Energy, Office of Science, Office of Basic Energy Sciences under Award No. 2008LANL 1026. W.Z.H. acknowledges N.T. Nuhfer's assistance with the PED method.

Received: ((will be filled in by the editorial staff))
Revised: ((will be filled in by the editorial staff))
Published online: ((will be filled in by the editorial staff))

[1] S.J. Zinkle, G.S. Was, *Acta Mater* 2013, *61,* 735.

[2] Y. Guerin, G.S. Was, S.J. Zinkle, *MRS Bull* 2009, *34,* 10.

[3] G.R. Odette, M.J. Alinger, B.D. Wirth, *Annu Rev Mater Res* 2008, *62*, 471.

[4]A. Misra, M.J. Demkowicz, X. Zhang, R. G. Hoagland *JOM* 2007, *59*, 62.

[5]L.K. Mansur, *Nucl Techol* 1978, 40, 5.

[6]B.N. Singh, A.J.E. Foreman, H. Trinkaus, *J Nucl Mater* 1997, *249*,107.

[7]M. Victoria, N. Baluc, C. Bailat, Y. Dai, M.I. Luppo, R. Schaublin, B.N. Singh, *J Nucl Mater* 2000*, 276*, 114.

[8]T.D. de la Rubia, H.M. Zbib, T.A. Khraishi, B.D. Wirth, M. Victoria, M.J. Caturla, *Nature* 2000, *406,* 871.

[9]B.D. Wirth, *Science* 2007, *318,* 923.

[10]J.R. Weertman, D. Farkas, K. Hemker, H. Kung, M. Mayo, R. Mitra, H. Van Swygenhoven. *MRS Bull* 1999, *24*, 44.

[11]Y.M. Wang, M.W. Chen, F.H. Zhou, E. Ma, *Nature* 2002, *419*,912.

[12]K.S. Kumar, H. Van Swygenhoven, S. Suresh, *Acta Mater* 2003, 51 (2003) 5743.

[13]J. Schiotz, K.W. Jacobsen, *Science* 2003,301,1357.

[14] Zhao YH, Liao XZ, Cheng S, Ma E, Zhu YT, *Adv Mater* 2006, *18*, 2280.

[15]Y. Chimi, A. Iwase, N. Ishikawa, A. Kobiyama, T. Inami, S. Okuda, *J Nucl Mater* 2001,*297* 355.

[16]T.D. Shen, S. Feng, M. Tang, J.A. Valdez, Y. Wang, K.E. Sickafus, *Appl Phys Lett* 2007, *90* 263115.

[17]R.W. Siegel, S.M. Chang, R.W. Balluffi, *Acta Metall* 1980, *28*, 249.

[18]S.J. Zinkle, K. Farrell, *J Nucl Mater* 1989, *168*, 262.

[19]X.M. Bai, A.F. Voter, R.G. Hoagland, M. Nastasi, B.P. Uberuaga, *Science* 2010, *327*, 1631.

[20]W.Z. Han, M.J. Demkowicz, E.G. Fu, Y.Q. Wang, A. Misra, *Acta Mater* 2012, *60,* 6341.

[21]M. Ames, J. Markmann, R. Karos, A. Michels, A. Tschope, R. Birringer, *Acta Mater* 2008, *56,* 4255.

[22]T. Chookajorn, H.A. Murdoch, C.A. Schuh, *Science* 2012, 337, 951.

[23]L. Lu, Y. Shen, X. Chen, L. Qian, K. Lu, *Science* 2004, *304*, 422.

[24]K. Lu, L. Lu, S. Suresh, *Science* 2009, *324*, 349.

[25]X. Zhang, A. Misra, *Scripta Mater* 2012, *66*, 860.

[26]M.J. Demkowicz, R.G. Hoagland, J.P. Hirth, *Phys Rev Lett* 2008, *100*, 136102.

[27]W.Z. Han, J.S. Carpenter, J. Wang, I.J. Beyerlein, N.A. Mara, *Appl Phys Lett* 2012, *100*, 011911.

[28]S.J. Zheng, I.J. Beyerlein, J.S. Carpenter, K. Kang, J. Wang, W.Z. Han, N.A. Mara, *Nature Communications* 2013, *4*,1696.

[29]S.B. Lee, J.E. LeDonne, S.C.V. Lim, I.J. Beyerlein, A.D. Rollett, *Acta Mater* 2012, *60*, 1747.

[30]Y. Saito, H. Utsunomlya, N. Tsuji, T. Sakai, *Acta Mater* 1999, *47*, 579.

[31]I.J. Beyerlein, N.A. Mara, J.S. Carpenter, T. Nizolek, W.M. Mook, T.A. Wynn, R.J. McCabe, J.R. Mayeur, K. Kang, S.J. Zheng, J. Wang, T.M. Pollock, *J Mater Res* 2013, *28*, 1799.

[32] M. Goken, H.W. Hoppel, *Adv Mater* 2011, *23*, 2663.

[33] M.J. Demkowicz, R.G. Hoagland, B.P. Uberuaga, A. Misra, *Phys Rev B* 2011, *84*, 104102.

[34]P. Moeck, S. Rouvimov, E.F. Rauch, M. Veron, H. Kirmse, I. Hausler, W. Neumann, D. Bultreys, Y. Maniette, S. Nicolopoulos, *Cry Res and Tech* 2011, *46*, 589.

[35]V. Tvergaard, *Adv Appl Mech* 1990, *27*, 83.

[36]M.J. Demkowicz, L. Thilly, *Acta Mater* 2011, *59*, 7744.

[37]K. Kang, J. Wang, I.J. Beyerlein, *J Appl Phys* 2012, *111,* 053531.

[38]J. F. Ziegler, J.P. Biersack, U. Littmark, *New York: Pergamon Press*; 1985.

Figure 1

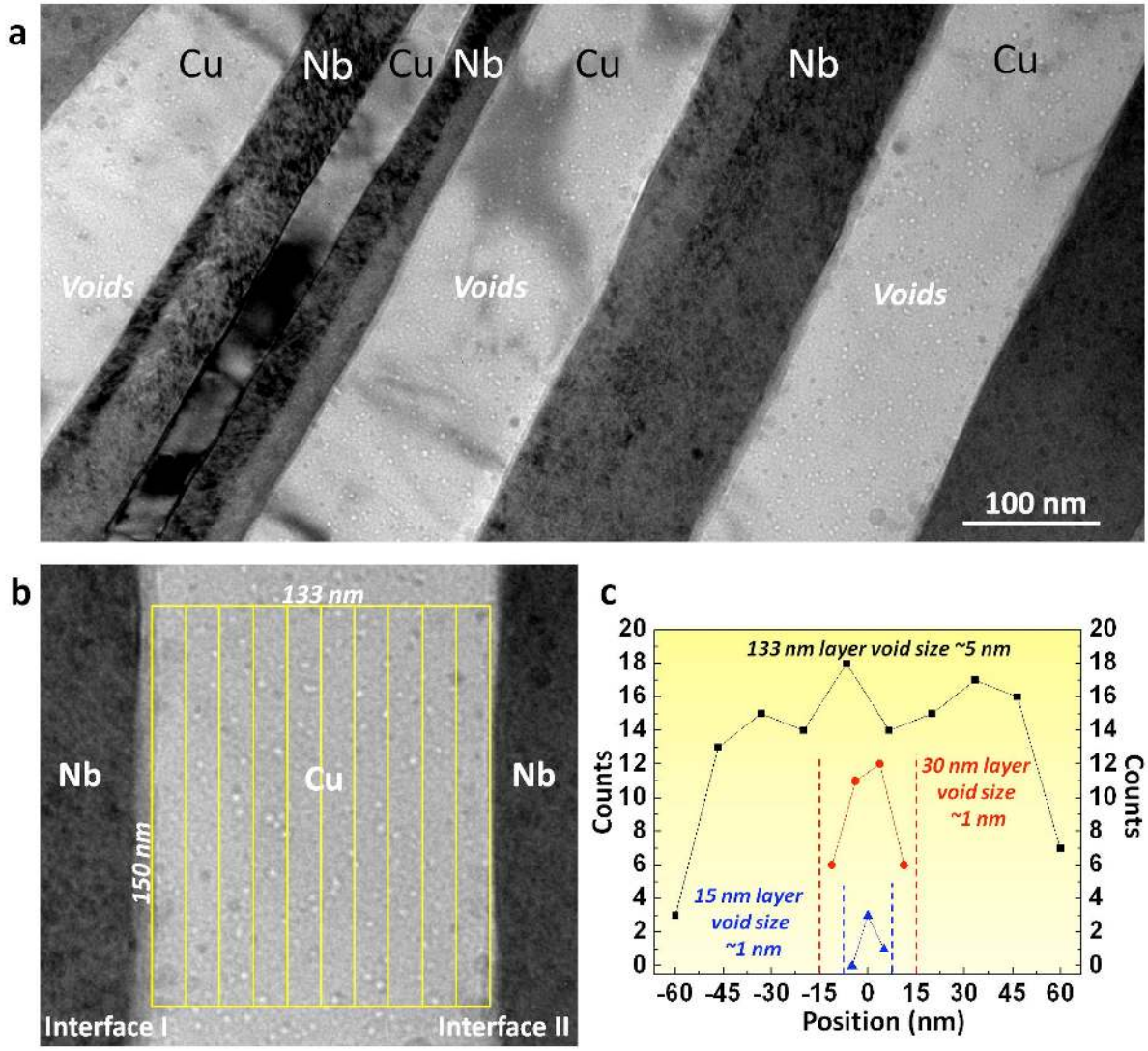

Figure 1. (a) Irradiation-induced voids in Cu layers in irradiated ARB NL Cu-Nb composites with 135 nm individual layer thickness. (b) Illustration of the method to determine the void number density in Cu layers. (c) Plot of the number density of voids as a function of distance from the center of the layer in 133 nm-, 30 nm-, and 15 nm-thick Cu layers. For each layer thickness, voids were counted over a 150 nm length of Cu layer.

Figure 2

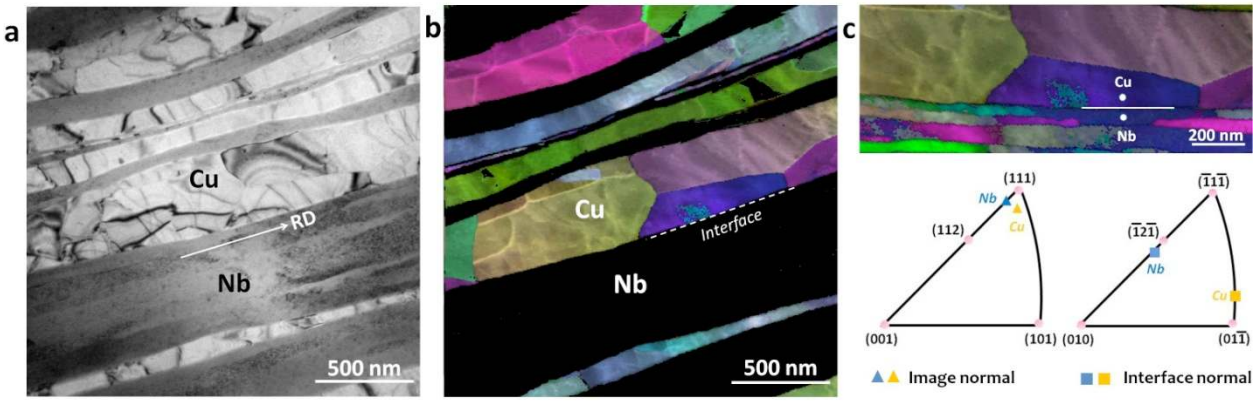

Figure 2. (a) Region of interest in a NL Cu-Nb composite observed by TEM (RD for rolling direction). (b) Interfaces are easily identified in a Cu phase orientation map. (c) Inverse pole figures show the image and interface plane normals extracted by PED for the indicated interface.

Figure 3

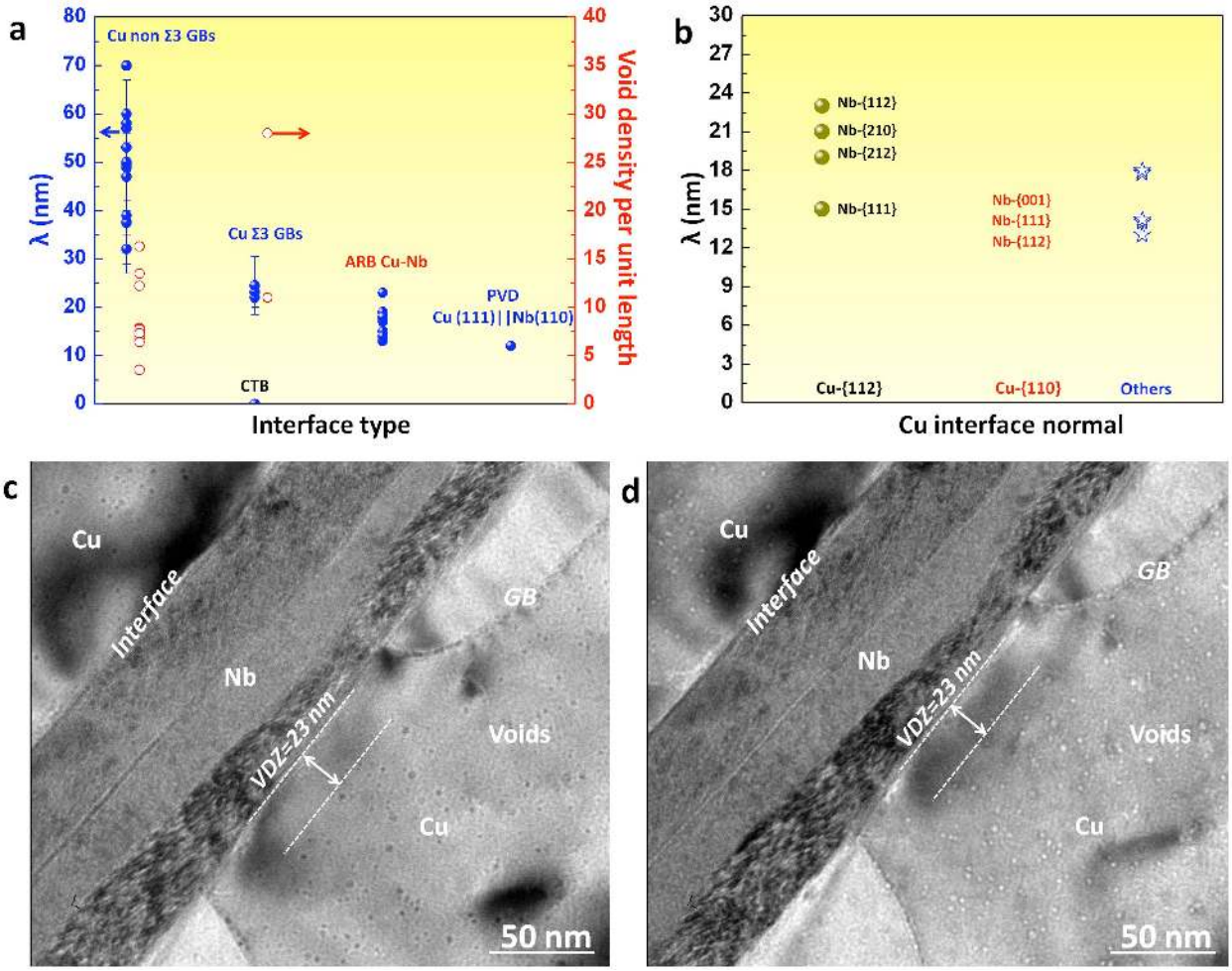

Figure 3. (a) Comparison of VDZ widths (λ) at Cu-Nb interfaces and at Cu GBs investigated under identical conditions[20]. (b) Widths of VDZs near Cu-Nb interfaces sorted by their plane orientations (labels use the nearest low index plane; see Table S1 and Fig. S4 for details). (c) Over-focus TEM image showing a VDZ near a Cu-Nb interface. (d) The same region imaged in under-focus.

Figure 4

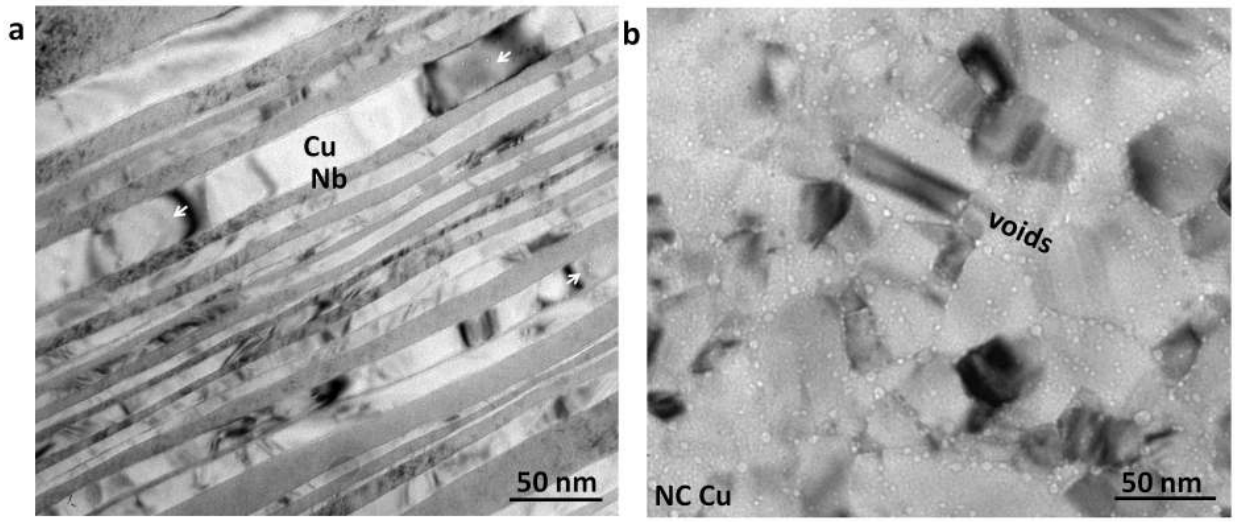

Figure 4. (a) Irradiated ARB NL Cu-Nb composites with 20 nm individual layer thickness are nearly void free. Arrows indicate small, isolated voids in the thicker Cu layers. (b) Irradiation damage in nanocrystalline Cu under identical conditions.

Supporting Information

for *Adv. Mater.*, DOI: 10.1002/adma.((please add manuscript number))

Design of Radiation Tolerant Materials via Interface Engineering

Weizhong Han, Michael J. Demkowicz, Nathan A. Mara, Engang Fu, Subhasis Sinha, Anthony D. Rollett, Yongqiang Wang, John S. Carpenter, Irene J. Beyerlein, Amit Misra

Figure S1-S5

Figure S1

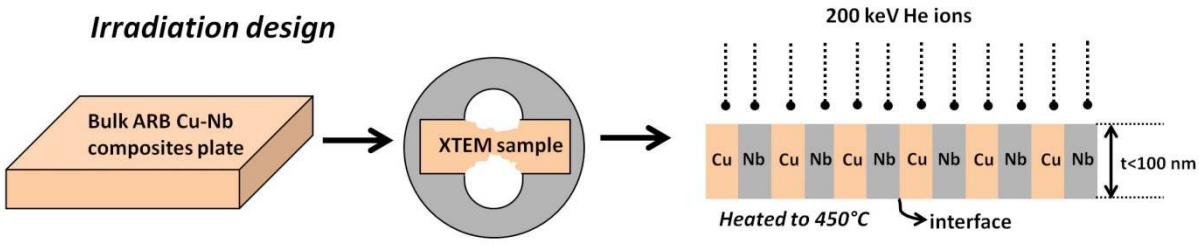

Figure S1. Schematic illustration of the He irradiation experimental procedures.

Figure S2

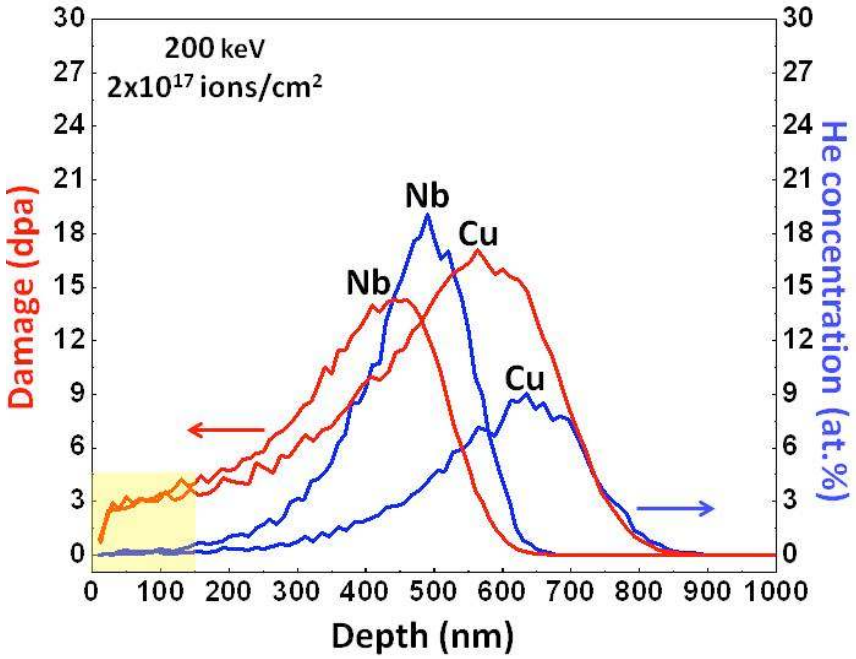

Figure S2. Depth profiles of damage (dpa) and implanted He concentration (at. %) computed using SRIM for a 200 keV He ion beam incident on pure Cu and pure Nb. During direct implantation on TEM foils of ARB Cu-Nb composites, the incident ion beam is parallel to the Cu-Nb interface (see Fig. S1). Thus, the damage level and He concentration may be estimated by using SRIM calculations on pure Cu and pure Nb. The yellow area in the figure indicates the uniform damage and near zero He concentration in the irradiated TEM foils.

Figure S3

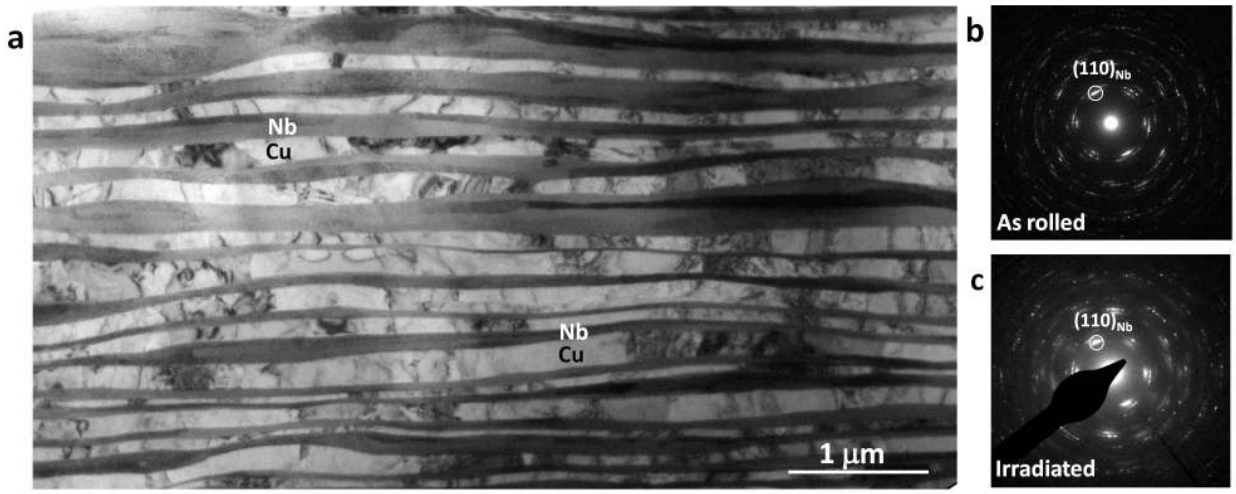

Figure S3. (a) Irradiated ARB NL Cu-Nb composites with 135 nm individual layer thickness; (b) Select area diffraction pattern (SADP) of as rolled ARB Cu-Nb composites; (c) SADP of irradiated ARB Cu-Nb composites.

Figure S4

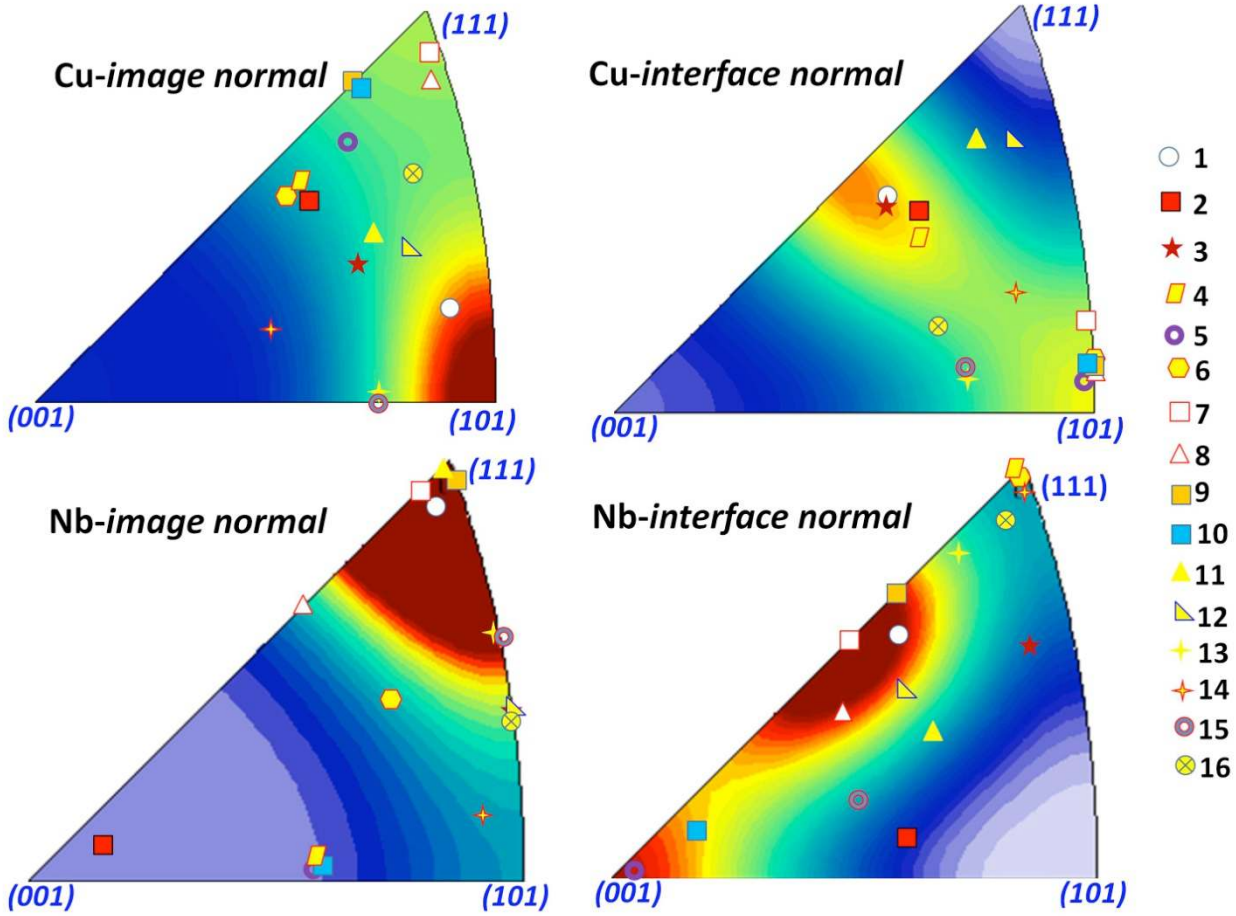

Figure S4. Interface orientation relationships measured by PED plotted on inverse pole figures of bulk texture measured by neutron diffraction (29). The Interface orientation relationship data plotted here are listed in Table S1.

Figure S5

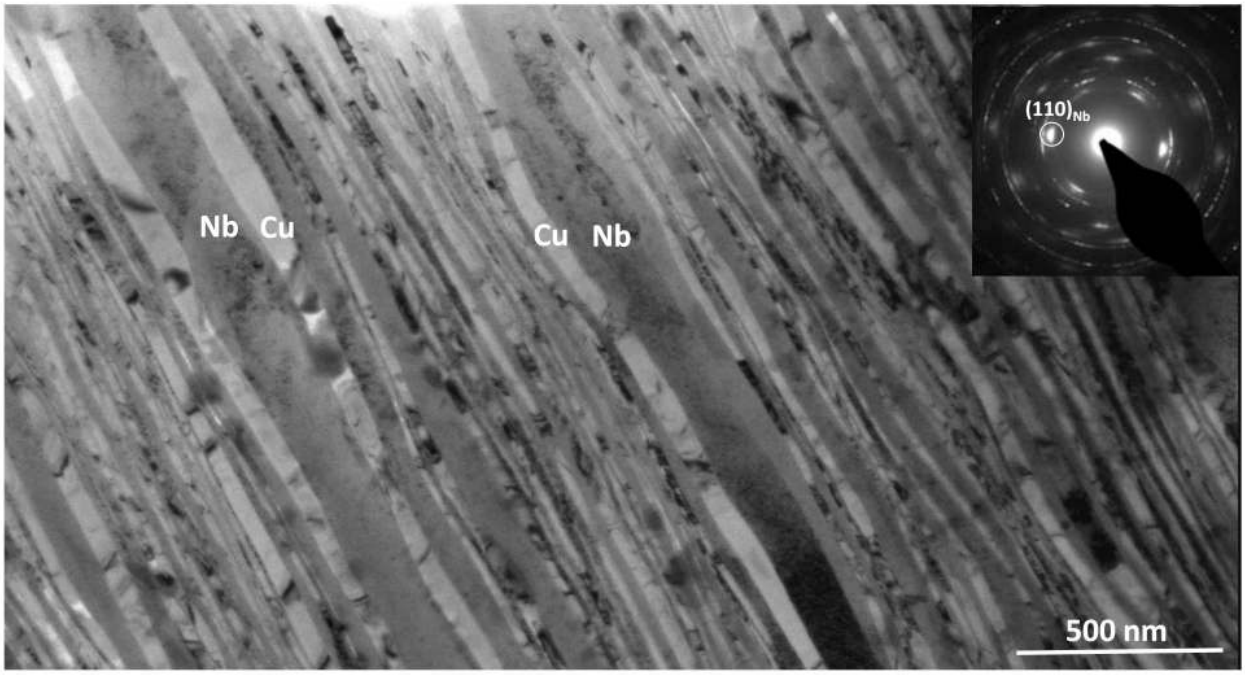

Figure 5S. Irradiated ARB NL Cu-Nb composites with 20 nm individual layer thickness and the corresponding SADP.

Table S1. List of interface orientation relationships measured by PED along with their VDZ widths. The numbers (No.) in first column are corresponding to the numbers in Fig. s4.

No.	Image normal	Interface plane	λ (nm)
1	Cu[20 4 23]//Nb[$\bar{1}2$ $\bar{1}1$ $\bar{1}4$]	Cu(10 25 $\bar{1}3$)//Nb($\bar{1}3$ 7 6)	23
2	Cu[11 8 21]//Nb[2 1 17]	Cu($\bar{9}$ $\bar{2}4$ 14)//Nb($\bar{1}5$ 8 1)	21
3	Cu[$\bar{7}$ $\bar{3}$ $\bar{1}1$]//Nb[3 1 3]	Cu(3 8 $\bar{4}$//Nb($\bar{1}3$ 6 11)	19
4	Cu[$\bar{1}0$ $\bar{8}$ $\bar{2}1$]//Nb[1 0 2]	Cu(23 7 $\bar{1}3$)//Nb($\bar{1}2$ $\bar{1}2$ 11)	15
5	Cu[13 11 21]//Nb[1 0 2]	Cu(21 $\bar{2}2$ $\bar{1}$//Nb($\bar{1}$ $\bar{3}0$ 0)	18
6	Cu[$\bar{1}0$ $\bar{8}$ $\bar{2}1$]//Nb[$\bar{2}$ $\bar{1}$ $\bar{3}$]	Cu(15 $\bar{1}5$ $\bar{1}$)//Nb($\bar{1}$ $\bar{1}$ $\bar{1}$)	15
7	Cu[8 7 9]//Nb[19 19 23]	Cu(11 2 $\bar{1}1$)//Nb($\bar{8}$ 19 $\bar{8}$)	15
8	Cu[$\bar{1}6$ $\bar{1}3$ $\bar{1}8$]//Nb[1 1 2]	Cu(21 2 $\bar{2}1$)//Nb($\bar{2}4$ 10 7)	14
9	Cu[2 2 3]//Nb[10 9 11]	Cu($\bar{1}9$ 19 1)//Nb(7 7 $\bar{1}3$)	11
10	Cu[2 2 3]//Nb[1 0 2]	Cu(10 $\bar{1}1$ 0//Nb($\bar{4}$ 29 2))	11
11	Cu[2 1 3]//Nb[1 1 1]	Cu(11 21 $\bar{1}5$)//Nb(4 $\bar{1}5$ 9)	18
12	Cu[$\bar{1}3$ $\bar{5}$ $\bar{1}7$]//Nb[$\bar{3}$ 1 3]	Cu(9 6 $\bar{1}1$//Nb($\bar{8}$ $\bar{2}4$ 13)	18
13	Cu[2 0 3]//Nb[$\bar{2}$ $\bar{1}$ $\bar{2}$]	Cu(18 $\bar{1}$ $\bar{1}2$)//Nb($\bar{1}3$ $\bar{1}4$ 20)	17
14	Cu[$\bar{1}0$ $\bar{3}$ $\bar{2}3$]//Nb[$\bar{8}$ $\bar{1}$ $\bar{9}$]	Cu(18 $\bar{2}3$ $\bar{5}$)//Nb($\bar{1}6$ $\bar{1}8$ 15)	14
15	Cu[2 0 3]//Nb[$\bar{2}$ $\bar{1}$ $\bar{2}$]	Cu(15 $\bar{1}$ $\bar{1}0$)//Nb($\bar{2}3$ 3 10)	14
16	Cu[$\bar{1}8$ $\bar{1}1$ $\bar{2}3$]//Nb[$\bar{3}$ 1 $\bar{3}$]	Cu(3 20 $\bar{1}2$)//Nb(11 12 $\bar{1}5$)	13
	Red: Cu interface normal close {112}	**Blue: Cu interface normal close {110}**	**Black: other**